

Learning based Age of Information Minimization in UAV-relayed IoT Networks

Biplav Choudhury *Student Member, IEEE*, Prasenjit Karmakar, Vijay K. Shah *Member, IEEE*, and Jeffrey H. Reed *Fellow, IEEE*

Abstract—Unmanned Aerial Vehicles (UAVs) are used as aerial base-stations to relay time-sensitive packets from IoT devices to the nearby terrestrial base-station (TBS). Scheduling of packets in such UAV-relayed IoT-networks to ensure fresh (or up-to-date) IoT devices’ packets at the TBS is a challenging problem as it involves two simultaneous steps of (i) *sampling* of packets generated at IoT devices by the UAVs [hop-1] and (ii) *updating* of sampled packets from UAVs to the TBS [hop-2]. To address this, we propose Age-of-Information (AoI) scheduling algorithms for two-hop UAV-relayed IoT-networks. First, we propose a low-complexity AoI scheduler, termed, *MAF-MAD* that employs Maximum AoI First (MAF) policy for sampling of IoT devices at UAV (hop-1) and Maximum AoI Difference (MAD) policy for updating sampled packets from UAV to the TBS (hop-2). We prove that *MAF-MAD* is the optimal AoI scheduler under ideal conditions (lossless wireless channels and generate-at-will traffic-generation at IoT devices). On the contrary, for general conditions (lossy channel conditions and varying periodic traffic-generation at IoT devices), a deep reinforcement learning algorithm, namely, Proximal Policy Optimization (PPO)-based scheduler is proposed. Simulation results show that the proposed PPO-based scheduler outperforms other schedulers like *MAF-MAD*, *MAF*, and round-robin in all considered general scenarios.

Index Terms—UAV, IoT Networks, Age of Information, DQN, PPO, Reinforcement Learning

I. INTRODUCTION

With their flexibility and low cost of deployment, Unmanned Aerial Vehicles (UAVs) are being increasingly used as fixed aerial base stations to monitor and collect data from Internet of Things (IoT) devices. Such a scenario has applications in (i) extending the coverage of the existing terrestrial base stations (TBSs) to IoT networks outside their direct wireless coverage [1], (ii) offloading data processing task to the TBS equipped with an edge server [2] etc. The UAVs act as a relay connecting the IoT devices and the TBS, and such communication networks are termed *UAV-relayed* IoT networks. An example is the smart city plans in Las Vegas where multiple UAVs are being deployed as “advanced contextual and situational awareness modules” to monitor and assess the data captured by IoT devices [3].

Scheduling of information packets in such UAV-relayed IoT networks becomes critical as it has to ensure that the

information received at the TBS from the IoT devices is timely or *fresh* [4]. The freshness of information is measured using the metric called “Age of Information” (AoI). AoI was first coined in the seminal work [5] and has received significant interest from the research community for time-sensitive networks. A detailed survey for AoI related works is presented in [6] and an online bibliography can be found in [7]. AoI is calculated at the receiver as the time elapsed since the most recently received information was generated at the source. It differs from traditional metrics such as latency, at lower network layers (transport, network, or link layer), which only focuses on the elapsed time for delivering information between two end nodes in a network.

AoI has been investigated for UAV networks, general IoT networks, vehicular networks, and other time-sensitive applications [8]–[11]. However, the communication in such networks are over a single hop and cannot be applied for the UAV-relayed IoT networks. UAV-relayed IoT network involves two hops where the first hop is from the IoT devices to the UAV providing them wireless coverage, and the second hop is from the UAVs to the TBS. Scheduling in such networks is different from single-hop networks as scheduling in two-hop networks will involve two time-ordered steps – (i) *sampling* of packets generated at the IoT devices by the UAVs, and (ii) *updating* of sampled packets from the UAVs to the TBS. Hence the scheduling for two-hop UAV relayed IoT networks is a non-trivial problem and is the focus of this work.

Moreover, existing AoI works mostly assumes (i) *non-lossy channel conditions* - in reality, wireless channels are lossy due to various factors and channel qualities change rapidly which must be taken into consideration while scheduling (ii) *generate-at-will* traffic generation model at IoT devices – on the contrary, IoT devices usually follow periodic traffic generation model, where an IoT device generates status updates at certain fixed periodic time intervals, which may be unknown apriori [12]. In this work, we investigate designing optimal scheduling policies for two-hop UAV-relayed IoT networks under general conditions¹. Specifically, we consider – (i) lossy channel conditions for both hops and, (ii) each IoT device generate packets at periodic traffic generation models, which is unknown to the scheduler.

The main contributions of this paper are the following-

- This paper investigates designing AoI scheduling policies for two-hop UAV-relayed IoT networks, which involves two time-ordered steps – (i) *sampling* of information

¹A preliminary version of this work has appeared in IEEE MASS 2021 [13].

Biplav Choudhury and Jeffrey H. Reed are with ECE Department at Virginia Tech. Prasenjit Karmakar is an independent researcher, and Vijay K. Shah is with Cybersecurity Engineering Department at George Mason University. (emails: {biplavc, reedjh}@vt.edu, prasenjitkarmakar52282@gmail.com and vshah22@gmu.edu). This research was supported in part by ONR under MURI Grant N00014-19-1-2621 and by Virginia Commonwealth Cyber Initiative (CCI). CCI is an investment in the advancement of cyber R&D, innovation, and workforce development (www.cyberinitiative.org).

packets from IoT devices to the UAV relay, and (ii) *updating* of sampled information packets (corresponding to each IoT device) from a UAV relay to the TBS.

- We first present a Maximal AoI First - Maximal AoI Difference (MAF-MAD) scheduling policy. Specifically, the MAF-MAD scheduler prioritizes sampling of an IoT device by the UAV relay which has highest AoI at the UAV relay, and similarly, updates the sampled information packet (at UAV relay) of the device with the highest AoI difference between the UAV and the TBS. We show that MAF-MAD is the optimal AoI scheduler under *ideal* conditions, which are characterized by non-lossy channel conditions and generate-at-will traffic generation models at the IoT devices.
- To design a scheduler for general conditions, we propose to leverage emerging reinforcement learning (RL) techniques which delivers superior performance in solving learning tasks even without any domain knowledge. We utilize an action-critic method, known as Proximal Policy Optimization (PPO) to design a scheduler that significantly outperforms the MAF-MAD scheduler under general conditions, i.e., channels are lossy and IoT devices follow periodic traffic generation models. This is because the neural network can learn the wireless network characteristics, i.e., channel fluctuations and IoT traffic generation models. We develop a novel voting mechanism which can efficiently capture the large action space in a smaller dimension. The PPO-based scheduler utilizes this voting approach and works well with larger network sizes and also, adapts well to changing network environments.
- Our simulation results show that the PPO-based scheduler outperform all considered baseline schedulers, namely, MAF-MAD, MAF, Round Robin (RR) and random schedulers under all considered simulation scenarios.

The rest of the paper is arranged as follows: Sec. II discusses the related works and Sec. III provides the system model for our work. In Sec. IV, we explain the different schedulers and their performance in minimizing AoI is presented in Sec. V. The paper is concluded in Sec. VI.

II. RELATED WORK

As the availability and ease of deployment of UAVs continue to improve, its role in IoT networks under the context of information freshness has seen great interest in recent years. In [14], the authors study a scenario where a single battery constrained UAV monitors multiple ground nodes. A deep learning based approach was used to develop a joint trajectory and scheduling design that minimizes AoI at the UAV. The work in [15] considers a scenario where a UAV has to visit multiple sensor nodes under battery constraints, while [16] considers a similar setting where a UAV has to sample information from multiple sensor nodes and report them to a data center. Similarly, a framework for finding the trajectory that minimizes the average and maximum AoI is presented in [17]. A cellular Internet of UAVs is considered in [18] where a distributed trajectory selection framework is proposed to minimize AoI. The authors in [8] propose a trajectory

finding algorithm that jointly optimizes energy transfer and data collection in an wireless powered environment. Note all these works along with [19]–[22] focus mainly on determining the optimal trajectory of the UAVs with the scheduling of packets being only over one hop from IoT devices to the UAV. Finally in [23], the optimal modulation and height to collect information from an energy-constrained sensor by a single UAV is investigated.

Since our UAV-relayed IoT network employ UAV as relays between IoT devices and the TBS, we also discuss the related works on AoI for relay networks. Authors in [24] consider a scenario with a single node transmitting to multiple nodes via relays. The source waits for an acknowledgment before transmitting the next sample, and the best waiting time is obtained in closed form. Reference [25] proposes optimal AoI minimizing online and offline policies where a single energy constrained source transmits its information to a single receiver via an energy constrained relay. In [26], a discrete-time stochastic hybrid system analysis is done, first under one relay and a direct link, and then with two relays and no direct link between a single transmitter and a single receiver. Our work is closest to [27] and [28]. In [27], a relay is used to sample and forward the information of multiple IoT devices to multiple destinations, and in [28], static UAVs hover above a highway to collect and forward packets from vehicles to a TBS. However, [27] considers a generate-at-will traffic model at the IoT devices with only a single UAV acting as the relay and [28] considers a fixed Poisson distribution based traffic generation at the vehicles.

III. SYSTEM MODEL AND PROBLEM FORMULATION

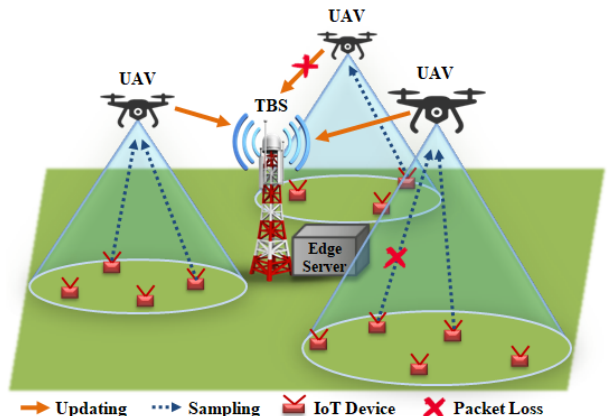


Fig. 1: Overview of UAV-relayed IoT networks

A. Network Model

As shown in Fig. 1, a UAV-relayed IoT network comprises of a terrestrial base station (TBS), M IoT devices and N UAVs. The TBS is located at a fixed 2D ground location and it is equipped with an edge server to process the collected time-sensitive information. M IoT devices are distributed randomly [29] in the considered region. We consider that the IoT devices are energy-constrained and have limited wireless range², and

²Most IoT devices have a wireless range of less than 100 meters [30].

are thus outside the wireless coverage of the nearby TBS, such as, in case of rural agricultural smart farms, where the IoT devices are far away from the nearest TBS. Therefore N UAVs are deployed as fixed aerial base stations (ABS) in the geographical region and act as *communication relays* between the nearby TBS and all M IoT devices. Each UAV $n \in N$ is deployed in the region of interest such that

(i) UAV n lies within the wireless coverage of the TBS and, provides *backhaul links* between itself and TBS and

(ii) UAV n provides wireless coverage as *access links* to m_n subset of IoT devices, where $m_n \subseteq M$.

Next we discuss different traffic generation models at each IoT device and the wireless channels considered in our model. Assume T is the total observation duration and it is divided into equal-length time slots denoted by t .

Traffic generation at the IoT devices. We consider two different types of traffic generation models at each IoT device m – (i) *generate-at-will*: device m generates new packet whenever it is selected to sample [14], and (ii) *periodic packet generation*: device m generates information packets at a fixed time interval denoted by its periodicity p_m . It means, m generates a new packet at slots $p_mt, 2p_mt, \dots, \lfloor \frac{T}{p_m} \rfloor t$. Note that though p_m is a fixed value for a certain IoT device m , it is unique to each IoT device, i.e., $p_m \neq p_{m'}$, where $m, m' \in M$. The scheduler doesn't have any prior information on the periodicity of traffic generation at the IoT devices. In certain scenarios the devices may change their periodicities. For example, a device may start generating packets at a faster/slower rate in response to application demands at the TBS, or network functions and protocols [31].

Channels: Let K denote the number of channels for communication between the TBS and all N UAVs. Similarly, let L_n denote the total number of channels available between a certain UAV n and its associated IoT devices. While our model can be easily extended to unique L_n channels for access links between a UAV and its associated IoT devices, we consider a fixed $L = L_n, (\forall n \in N)$ channels for access links between a certain UAV and its associated IoT devices for ease of presentation. Even though a certain IoT device may fall within the wireless coverage of two or more UAVs, we assume that each IoT device is associated to a unique UAV based on an association policy (e.g., max power association policy [32]), and thus, the subset of IoT devices, m_n , is unique to each UAV, and $M = \cup_{i=1}^N m_i$.

Under ideal channel conditions, it can be assumed that there is neither intra-cell interference (i.e., UAV and its associated IoT devices) nor inter-cell interference (i.e., UAV to UAV). This is realistically possible by employing non-overlapping orthogonal channels for both access links [33] and backhaul links [34]. This results in the channels being lossless so that no packet drops occur.

However, under general channel conditions, link outages [35] occurring due to noise, interference or other factors can cause packet loss at the channels. These link outages are captured by considering that the link between device m and the associated UAV n_m has a non-zero probability of dropping the transmitted packets [13], [27], [36], which we refer to as, *Sample Loss Probability* and is denoted by $l_{s,m} \in (0, 1)$.

Similarly, $l_{u,m} \in (0, 1)$ denotes the *Update Loss Probability*, which refers to the packet loss probability between UAV n_m and the TBS. While our approach can be used for any channel model, we pre-assign an expected loss probability for ease of reproducibility [13], [27], [36].

Note that (UAV-IoT) communication channels (L) and (TBS-UAV) communications channels (K) are termed as *UAV channels* and *TBS channels* respectively, for ease of presentation in rest of the paper. Also, notice that the **ideal** network condition refers to not only (i) both UAV and TBS channels being ideal (or non-lossy), but also, (ii) the IoT devices generate information packets using *generate-at-will* packet generation model. On contrary, the **general** condition means UAV and TBS channels are lossy and the IoT devices follow periodic packet generation model.

Scheduling: At each slot t , our considered UAV-relayed IoT networks involves two simultaneous scheduling steps – (i) *sampling* of packets generated at the IoT devices by the UAVs, and (ii) *updating* of sampled packets from the UAVs to the TBS. The set of IoT devices sampled by UAV n is denoted by $S_n(t)$ and total devices sampled by all the UAVs is $\mathcal{S}(t) = \{\mathcal{S}_1(t), \mathcal{S}_2(t), \dots, \mathcal{S}_N(t)\}$. Similarly, updated devices are denoted as $\mathcal{U}(t)$. When a device m is sampled, it transmits its most recent packet to the serving UAV n_m and it will replace any of its older packet at n_m [36]. Then when it is updated, the packet is transmitted from UAV n_m to the TBS. At any slot, each channel can support at most 1 packet.

B. Age of Information (AoI) at the UAV and TBS

We employ Age of Information (AoI) to measure the freshness of information. In particular, AoI is defined as *time elapsed since the generation time of the most-recent packet received (by the UAV/TBS in our case)*.

The AoI of IoT device m at UAV n_m is denoted as

$$AoI_m^{UAV}(t) = t - \tau_{s,m} \quad (1)$$

where t is the current slot and $\tau_{s,m}$ is the generation time of the *most recently sampled* packet of device m that was received successfully at UAV n_m . Similarly, the AoI of device m at the TBS is

$$AoI_m^{TBS}(t) = t - \tau_{u,m} \quad (2)$$

where $\tau_{u,m}$ is the generation time of the *most recently updated* packet of the m th IoT device that was received successfully at the TBS. Based on Eqn. (1) and (2), AoI increases linearly in slots of no reception and decreases at reception instants.

The evolution of AoI with time at the UAVs and TBS is described next. At t , if device m was selected for sampling, i.e., $m \in \mathcal{S}(t)$, its AoI at the UAV changes as

$$AoI_m^{UAV}(t+1) = \begin{cases} t+1 - \tau_{s,m} & \text{with prob. } 1 - l_{s,m} \\ AoI_m^{UAV}(t) + 1 & \text{with prob. } l_{s,m} \end{cases} \quad (3)$$

Else if the device m was not sampled, i.e., $m \notin \mathcal{S}(t)$, its AoI at the UAV changes as

$$AoI_m^{UAV}(t+1) = AoI_m^{UAV}(t) + 1 \quad (4)$$

Similarly AoI for IoT device m at the TBS when selected for update such that $m \in \mathcal{U}(t)$ and when not selected for update such that $m \notin \mathcal{U}(t)$ are shown in Eqn. (5) and (6).

$$AoI_m^{TBS}(t+1) = \begin{cases} AoI_m^{UAV}(t) + 1 & \text{with prob. } 1 - l_{u,m} \\ AoI_m^{TBS}(t) + 1 & \text{with prob. } l_{u,m} \end{cases} \quad (5)$$

$$AoI_m^{TBS}(t+1) = AoI_m^{TBS}(t) + 1 \quad (6)$$

Thus a device's AoI increases at the UAVs and the TBS if-

- it was sampled/updated but the packet was lost
- it was not sampled/updated.

As the information is relayed through the UAVs, AoI_m^{UAV} directly impacts AoI_m^{TBS} . Note that the communication between a device and the TBS has a delay of a single slot, due to which information sampled by an UAV at a certain slot cannot be updated to the TBS in the same slot [13], [27].

Finally, the average AoI of all IoT devices at the UAVs and the TBS during the observation interval T is calculated as Eqn. (7) and (8) respectively

$$AoI^{UAV}(T) = \frac{1}{TM} \sum_{t=1}^T \sum_{m=1}^M AoI_m^{UAV}(t) \quad (7)$$

$$AoI^{TBS}(T) = \frac{1}{TM} \sum_{t=1}^T \sum_{m=1}^M AoI_m^{TBS}(t) \quad (8)$$

Problem formulation: Our objective is to design a scheduler that ensures minimum AoI corresponding to all IoT devices at the TBS. Given $\mathcal{S}_n(t)$ and $\mathcal{U}(t)$ respectively denote the set of the IoT devices sampled by each UAV $n \in N$ and updated to the TBS at a certain slot $t \in T$, we formulate the AoI-aware scheduling problem as the minimization of the average AoI of all IoT devices at the TBS (Eqn. (8)) subject to the limited channel constraints, as follows.

$$\min AoI^{TBS}(T)$$

$$\text{s.t. } |\mathcal{S}_n(t)| \leq L, \quad \forall n \in N \text{ and } t = 1, 2 \dots T \quad (9)$$

$$|\mathcal{U}(t)| \leq K, \quad t = 1, 2 \dots T \quad (10)$$

where constraint (9) and (10) refers to the limited number of channels for the sampling and updating respectively. The notations used in this paper are summarized in Table I.

IV. SCHEDULING POLICIES

We first propose a simple low-complexity *Maximal AoI First-Maximal AoI Difference* (MAF-MAD) scheduling algorithm to solve the above problem. MAF-MAD is a centralized algorithm and runs at the TBS and its underlying idea is to sample devices with maximum AoI at the serving UAV, and update IoT devices with maximum AoI difference between the UAV and the TBS. We show that MAF-MAD is an

TABLE I: Notations

Meaning	Symbol
Number of IoT devices	M
Number of UAVs	N
IoT devices associated to UAV n	m_n
UAV providing coverage to device m	n_m
Packet generation periodicity of device m	p_m
AoI of device m at UAV	AoI_m^{UAV}
AoI of device m at TBS	AoI_m^{TBS}
Packet loss between device m and UAV n_m	$l_{s,m}$
Packet loss between device m and TBS	$l_{u,m}$
Devices sampled at t by UAV n	$\mathcal{S}_n(t)$
Devices sampled at $t = \{\mathcal{S}_1(t), \mathcal{S}_2(t), \dots, \mathcal{S}_N(t)\}$	$\mathcal{S}(t)$
Devices updated at t	$\mathcal{U}(t)$
Channels at each UAV	L
Channels at the TBS	K

optimal scheduler for UAV-relayed IoT networks under **ideal conditions** where (i) *the channels are non-lossy* and (ii) *all the IoT devices follow generate-at-will traffic generation models*. However, under **general conditions** where the *wireless channels are lossy* and *the IoT device follow periodic traffic generation models*, the scheduling decisions need to incorporate practical problems of packet generation instants and channel non-idealities, which is not possible in case of MAF-MAD scheduler. Thus, we design a PPO-based centralized scheduler which will learn the unique network characteristics and thus, promises to perform well for UAV-relayed IoT networks under general conditions.

A. MAF-MAD Scheduler

The Maximal AoI First - Maximal AoI Difference (MAF-MAD) scheduler is presented in Algorithm 1. At any time $t \in T$, the inputs to the this algorithm are AoI of each IoT device $m \in M$ at its serving UAV $AoI_m^{UAV}(t)$ and at the TBS $AoI_m^{TBS}(t)$. For the sampling step in line 3, each UAV n samples L IoT devices with the maximal AoI, $AoI_m^{UAV}(t)$ from the m_n IoT devices associated with it based on a maximal AoI first (MAF) policy. Note that ideally we should consider AoI difference between the UAV and the IoT device, but this is not feasible as the scheduler doesn't know the traffic generation instants of the IoT devices. However when devices generate packets using generate-at-will traffic model, any device which is selected to be sampled will generate a new packet at that slot due to which $AoI_m^{UAV}(t)$ also becomes the AoI difference between the UAV and the IoT device.

Then for the updating step, devices with *maximal AoI difference* (MAD) between the UAV and TBS are prioritized. This AoI difference is calculated as

$$AoI_m^{diff}(t) = AoI_m^{TBS}(t) - AoI_m^{UAV}(t) \quad (11)$$

where $AoI_m^{TBS}(t) \geq AoI_m^{UAV}(t)$. The TBS updates K devices out of the total M IoT devices with the highest $AoI_m^{diff}(t)$, as shown in line 5.

Theorem IV.1. *Under ideal conditions, i.e., no lossy channels and generate-at-will sampling at IoT devices, MAF-MAD is the optimal scheduling policy for minimizing average AoI at the TBS for status updates generated at each IoT device.*

Algorithm 1 MAF-MAD scheduler

Input: $AoI_m^{UAV}(t)$ and $AoI_m^{TBS}(t)$ for $m \in M$.

Output: $\mathcal{S}(t), \mathcal{U}(t)$.

- 1: $\mathcal{S}(t) = \phi$
 - 2: **for** UAV $n = 1, 2, \dots, N$ **do**:
 - 3: $\mathcal{S}_n(t) = \arg \max_{S \subseteq m_n, |S_n(t)| \leq L} \{AoI_m^{UAV}(t)\}_{m=1}^{m_n}$
 - 4: $\mathcal{S}(t) = \mathcal{S}(t) \cup \mathcal{S}_n(t)$
 - 5: $\mathcal{U}(t) = \arg \max_{U \subseteq M, |U(t)| \leq K} \{AoI_m^{diff}(t)\}_{m=1}^M$
-

Proof. As presented in [27], to minimize the AoI at a destination ($AoI^{TBS}(T)$ in our case), at each slot $t = 1, 2, \dots, T$ the optimal scheduler needs to

- sample devices whose packet reception at the relay (UAV in our case) will lead to the maximum reduction of average AoI at the relay,
- update devices whose packet reception at the TBS will lead to the maximum reduction of average AoI at TBS.

We first show that sampling as per MAF-MAD offers the maximum reduction in average AoI at all the UAVs.

AoI reduction at the UAVs: Consider a UAV n providing coverage to $|m_n|$ (out of M) IoT devices. At slot t , the average AoI of these IoT devices at UAV n is

$$AoI_n^{UAV}(t) = \frac{1}{Tm_n} \sum_{i=1}^{m_n} AoI_i^{UAV}(t) \quad (12)$$

and from the result cited above, the optimal scheduler will sample those devices which will lead to maximum reduction of average AoI at n from $AoI_n^{UAV}(t)$ to $AoI_n^{UAV}(t+1)$.

For simplicity, assume $L=K=1$. Therefore the scheduler needs to select $L=1$ device to sample. Let device $j \in m_n$ have the largest AoI at n such that $AoI_j^{UAV}(t) = \max(AoI_1^{UAV}(t), AoI_2^{UAV}(t), \dots, AoI_{m_n}^{UAV}(t))$. From Algorithm 1 step 3, at t the MAF-MAD scheduler will sample the j th device. Then the reduction in the average AoI at n is

$$\begin{aligned} \Delta AoI_n^{UAV}(t+1) &= \frac{1}{Tm_n} (AoI_n^{UAV}(t) - AoI_n^{UAV}(t+1)) \\ &= \frac{1}{Tm_n} \sum_{i=1}^{m_n} (AoI_i^{UAV}(t) - AoI_i^{UAV}(t+1)) \end{aligned} \quad (13)$$

For the $|m_n| - 1$ unsampled devices, their $AoI^{UAV}(t+1)$ increases by 1 (Eqn. (4)). $AoI^{UAV}(t+1)$ for j becomes $t + 1 - \tau_{s,m}$ as per Eqn. (3) under no packet loss. Additionally for generate-at-will, j will generate a packet at t , i.e., $\tau_{s,m} = t$, as it was sampled at t . Therefore Eqn. (13) becomes

$$\begin{aligned} \Delta AoI_n^{UAV}(t+1) &= \frac{1}{Tm_n} \left(\sum_{i=1, i \neq j}^{|m_n|} (AoI_i^{UAV}(t) - AoI_i^{UAV}(t+1)) + (AoI_j^{UAV}(t) - AoI_j^{UAV}(t+1)) \right) \\ &= \frac{1}{Tm_n} (-(|m_n| - 1) + AoI_j^{UAV}(t) - (t+1-t)) \\ &= \frac{1}{Tm_n} (AoI_j^{UAV}(t) - |m_n|) \end{aligned} \quad (14)$$

Now for any other scheduler that selects device j' to sample where $j' \neq j$ and hence $AoI_{j'}^{UAV}(t) > AoI_j^{UAV}(t)$, the reduction in AoI at n will be given by

$$\Delta' AoI_n^{UAV}(t+1) = \frac{1}{Tm_n} (AoI_{j'}^{UAV}(t) - |m_n|) \quad (15)$$

Now comparing Eqn. (14) and (15), $\Delta AoI_n^{UAV}(t+1) > \Delta' AoI_n^{UAV}(t+1)$. Because all the UAVs $n \in N$ operate independently, the same result holds for other UAVs too. Hence the MAF-MAD scheduler offers the largest AoI reduction at all the UAVs in the sampling step.

AoI reduction at the TBS: In the updating step, the scheduler needs to select $K=1$ device to update. From Algorithm 1 step 5, at t the MAF-MAD scheduler will update the k th device such that $AoI_k^{diff}(t) = \max(AoI_1^{diff}(t), AoI_2^{diff}(t), \dots, AoI_M^{diff}(t))$. After the update, the reduction in average AoI at the TBS is

$$\begin{aligned} \Delta AoI^{TBS}(t+1) &= \frac{1}{TM} (AoI^{TBS}(t) - AoI^{TBS}(t+1)) \\ &= \frac{1}{TM} \left(\sum_{i=1}^M (AoI_i^{TBS}(t) - AoI_i^{TBS}(t+1)) \right) \\ &= \frac{1}{TM} \left(\sum_{i=1}^M (AoI_i^{TBS}(t) - AoI_i^{TBS}(t+1)) \right) \end{aligned} \quad (16)$$

For $M-1$ devices that were not updated, their $AoI^{TBS}(t+1)$ increases by 1 (Eqn. (6)). $AoI^{TBS}(t+1)$ for the updated device k will change as per Eqn. (5) when there is no packet loss. Therefore Eqn. (16) becomes

$$\begin{aligned} \Delta AoI^{TBS}(t+1) &= \frac{1}{TM} \left(\sum_{i=1, i \neq k}^M (AoI_i^{TBS}(t) - AoI_i^{TBS}(t+1)) + (AoI_k^{TBS}(t) - AoI_k^{TBS}(t+1)) \right) \\ &= \frac{1}{TM} (-(M-1) + AoI_k^{TBS}(t) - AoI_k^{TBS}(t+1)) \\ &= \frac{1}{TM} (-M+1 + AoI_k^{TBS}(t) - AoI_k^{UAV}(t) - 1) \\ &= \frac{1}{TM} (AoI_k^{diff}(t) - M) \end{aligned} \quad (17)$$

Now for any other scheduler that selects device k' to sample where $k' \neq k$ and hence $AoI_k^{diff}(t) > AoI_{k'}^{diff}(t)$, the reduction in average AoI at the TBS will be given by

$$\Delta' AoI^{TBS}(t+1) = \frac{1}{TM} (AoI_{k'}^{diff}(t) - M) \quad (18)$$

Comparing Eqn. (17) and (18), we see $\Delta AoI^{TBS}(t+1) > \Delta' AoI^{TBS}(t+1)$. Hence MAF-MAD also leads to the maximum reduction in $AoI^{TBS}(T)$. Therefore when there is no packet loss at any of the sampling and updating steps, and the devices generate traffic based on generate-at-will policy, MAF-MAD is the optimal scheduler for minimizing $AoI^{TBS}(T)$. \square

B. Proximal Policy Optimization (PPO) based scheduler

While the MAF-MAD scheduler provides the best AoI minimization under ideal conditions; however, as shown in our preliminary work [13] and also in Sec. V, it doesn't do well under general conditions with lossy channels and periodic packet generation at the IoT devices, both of which are unknown a priori at the scheduler. This motivates for a reinforcement learning (RL) based approach where the scheduler can learn these characteristics. In our preliminary work [13], we showed that while a DQN based scheduler works well for networks having small number of actions, it doesn't scale with network size. In this work, we propose an actor critic based approach, PPO, that is suitable for such scenarios. Details on the PPO scheduler and comparison between the PPO and DQN schedulers will be discussed in the upcoming sections.

1) *PPO Preliminaries*: In this section, we give a brief introduction to deep RL and PPO algorithm.

a) *Episode, Return, and Value function*: In RL, mathematical entities commonly known as agents, learn to make optimal decisions by interacting in an unknown environment and exploiting the received feedback. Usually, Markov Decision Process (MDP) is used to simulate such environment that requires decision making in situations where outcome is partly random and partly under the control of the decision maker or agent. MDP is formally defined as the tuple $\{\mathcal{X}, \mathcal{A}, \mathcal{T}, p(x_0), \gamma\}$. Therefore, the environment consists of a transition function $\mathcal{T} : \mathcal{X} \times \mathcal{A} \rightarrow p(\mathcal{X})$ and a reward function $\mathcal{R} : \mathcal{X} \times \mathcal{A} \times \mathcal{X} \rightarrow \mathbb{R}$. At slot t , the agent observe some state $x_t \in \mathcal{X}$ and picks an action $a_t \in \mathcal{A}$ with policy $\pi(a_t|x_t) : \mathcal{X} \rightarrow p(\mathcal{A})$. As a result, the environment transitions to a next state $x_{t+1} \sim \mathcal{T}(\cdot|x_t, a_t)$ and returns a scalar reward $r_t = \mathcal{R}(x_t, a_t, x_{t+1})$. The first state x_0 is sampled from the initial state distribution $p(x_0)$. Finally, $\gamma \in [0, 1]$ is the discount factor.

The agent interacts with the environment until it reaches the terminal state or reaches the time limit T , completing an episode $\tau = \{x_0, a_0, r_0, \dots, x_t, a_t, r_t, \dots, x_{T-1}, a_{T-1}, r_{T-1}, x_T\}$ ³. Thus quality of state x_t can be realized as the cumulative sum of rewards from x_t to the end of the episode τ , which is known as the return G_t , see Eqn. (19). However, due to the stochastic nature of the environment, there can be many possible next states x_{t+1} , resulting multiple return G_t values

from state x_t for different episodes. Therefore, quality of state x_t is defined by the value function $V(x_t)$, as the expected return from state x_t , see Eqn. (20).

$$G_t = \sum_{\hat{t}=t}^T \gamma^{\hat{t}-t} r_{\hat{t}} \quad (19)$$

$$V(x_t) = \mathbb{E}[G_t | x_t] \quad (20)$$

b) *Actor-Critic methods*: The primary objective of the agent is to behave optimally with policy $\pi(a_t|x_t)$ so that it can obtain a high cumulative reward $R_\tau = r_0 + r_1 + r_2 + \dots + r_{T-1}$ in episode τ . In stochastic policy gradient methods, we maximize the cost function $J(\pi) = \sum_{\tau=1}^{\infty} p(\tau) R_\tau$ with respect to the policy $\pi(a_t|x_t)$ to increase the likelihood of sampling the most rewarding episode, where $p(\tau)$ is the probability of sampling episode τ with current policy $\pi(a_t|x_t)$.

In practice, the state x_t can be multi-dimensional, making it infeasible for traditional table based RL approaches [37]. This provides a clear path for the application of universal function approximators (i.e, neural networks) to model policy $\pi(a_t|x_t)$ with parameter θ . Similarly, value function $V(x_t)$ is modeled with parameters ψ . The parameterized policy $\pi(a_t|x_t; \theta)$ and the value function $V(x_t; \psi)$ is commonly known as the **actor** and the **critic** networks respectively.

While the actor network interacts with the environment and collect experiences $\{x_t, a_t, r_t, x_{t+1}\}$, the advantage is computed as shown in Eqn. (21). Advantage A_t represents the incentive obtained by taking action a_t at state x_t from the prospective of the critic network. Subsequently, the actor and the critic network is jointly optimized by back-propagating the gradients from Eqn. (22) and Eqn. (23).

$$A_t = r_t + \gamma V(x_{t+1}; \psi) - V(x_t; \psi) \quad (21)$$

$$\nabla_{\theta} J(\theta) = \mathbb{E}[\nabla_{\theta} \log \pi(a_t|x_t; \theta) A_t] \quad (22)$$

$$\nabla_{\psi} \mathcal{L}(\psi) = \mathbb{E}[(G_t - V(x_t; \psi)) \nabla_{\psi} V(x_t; \psi)] \quad (23)$$

c) *Proximal Policy Optimization*: The actor-critic algorithms that rely on the policy gradient formulation suffer from divergent behavior unless we impose a mechanism to constrain the change of the actor's policy. The primary reason is the on-policy data collection for optimizing the actor and the critic network. This issue is addressed in [38] by introducing trust-region policy updates. Since then, actor-critic algorithms have excelled at tackling real-world problems due to their increased efficiency and stability with respect to Q-Learning. Proximal Policy Optimization (PPO) is the recent addition [39] to such class of algorithms and therefore inherits the aforementioned properties. Moreover, PPO improves the efficiency further and achieves trust-region policy updates by simply clipping the probability ratio $\zeta_t \in [1 - \epsilon, 1 + \epsilon]$ between the current $\pi(a_t|x_t; \theta)$ and the old $\pi(a_t|x_t; \theta_{old})$ actor policies. PPO optimizes the actor network with the gradients shown in Eqn. (24) and also leverages entropy $\mathcal{H}(\theta)$ based regularization to encourage exploration at early stages of learning. The **combined gradient** in Eqn. (25) optimizes the *actor* and the

³Observation interval T is much smaller than simulation duration \mathbb{T} .

critic networks simultaneously, where c_1, c_2 are constants.

$$\nabla_{\theta} J(\theta) = \mathbb{E} \left[\nabla_{\theta} \text{Min}(\zeta_t A_t, [\zeta_t]_{1-\epsilon}^{1+\epsilon} A_t) \right] \quad (24)$$

$$\text{where, } \zeta_t = \frac{\pi(a_t|x_t; \theta)}{\pi(a_t|x_t; \theta_{old})}$$

$$\nabla_{\theta \cup \psi} \mathcal{L}(\theta \cup \psi) = -\nabla_{\theta} J(\theta) + c_1 \nabla_{\psi} \mathcal{L}(\psi) - c_2 \nabla_{\theta} \mathcal{H}(\theta) \quad (25)$$

2) *MDP formulation*: In this section, we formulate the packet scheduling to minimize AoI at UAV-relayed IoT networks as an MDP. The state, action and reward in the context of our work is explained next.

a) *State Space*: State is the scenario encountered by the scheduler. At slot t , state is defined as

$$x_t = \{\hat{t}, \{AoI_m^{UAV}(\hat{t})\}_{m=1}^M, \{AoI_m^{TBS}(\hat{t})\}_{m=1}^M\}_{\hat{t}=t}^{t-z+1} \quad (26)$$

where z is the stacking size. The stacking size is discussed in Sec. V-B. At $t=1$, $AoI_m^{UAV}(t)$ and $AoI_m^{TBS}(t)$ are initialized to 1. The state space is denoted by \mathcal{X} .

b) *Action Space*: As described in Sec. III, scheduling involves two simultaneous steps of sampling and updating devices at each slot. Therefore the action at each slot t is

$$a_t = (\mathcal{S}(t), \mathcal{U}(t)) \quad (27)$$

where $\mathcal{S}(t) = \{S_1(t), S_2(t), \dots, S_N(t)\}$ is the set of all devices sampled by all the UAVs at slot t such that $|S_n(t)| \leq L \forall n \in N$. Similarly, $\mathcal{U}(t)$ is the set of devices selected to update their packets to the TBS where $|\mathcal{U}(t)| \leq K$. The action space is denoted by \mathcal{A} , where $|\mathcal{A}| = (\prod_i^{m_i} C_L) \times M C_K$.

c) *Reward*: As the objective is improving the information freshness at the TBS, the reward is given by the negative of the average AoI of all the devices at the TBS at slot $t+1$

$$r_t = \mathcal{R}(x_t, a_t, x_{t+1}) = -\frac{1}{M} \sum_{m=1}^M AoI_m^{TBS}(t+1) \quad (28)$$

Based on action a_t , the environment transitions from state x_t to a new state x_{t+1} according to the state transition probabilities described in Eqn. (3), (4), (5), (6) while resulting in a reward r_t . Thus it is a finite horizon MDP with finite state and action spaces, which makes it suitable for RL approaches.

3) *Voting mechanism*: Here, we propose the voting mechanism, which efficiently captures the action space \mathcal{A} for sampling and updating packets at UAV $n \in N$ and TBS respectively. The advantage of using voting to sample L packets from m_n devices at UAV $n \in N$ is following- at slot t , we compute votes $v_i^t \forall i \in m_n$ devices and sample packets from $S_n(t)$ devices with top L votes as shown in Eqn. (29). Hence, we can capture ${}^{m_n}C_L$ possible sampling actions with m_n votes. Similarly, we can update K packets to the TBS from M devices with Eqn. (30). The benefit of this approach will be clearer if we consider all N UAVs and the TBS, since we only have to compute $(\sum_{n=1}^N m_n) + M = 2M$ votes to represent an action space with cardinality $|\mathcal{A}| = (\prod_i^{m_i} C_L) \times M C_K$.

$$S_n(t) = \arg \max_{S' \subseteq m_n, |S'| \leq L} \{v_i^t\}_{i=1}^{m_n} \forall n \in N \quad (29)$$

$$\mathcal{U}(t) = \arg \max_{U' \subseteq M, |U'| \leq K} \{v_i^t\}_{i=1}^M \quad (30)$$

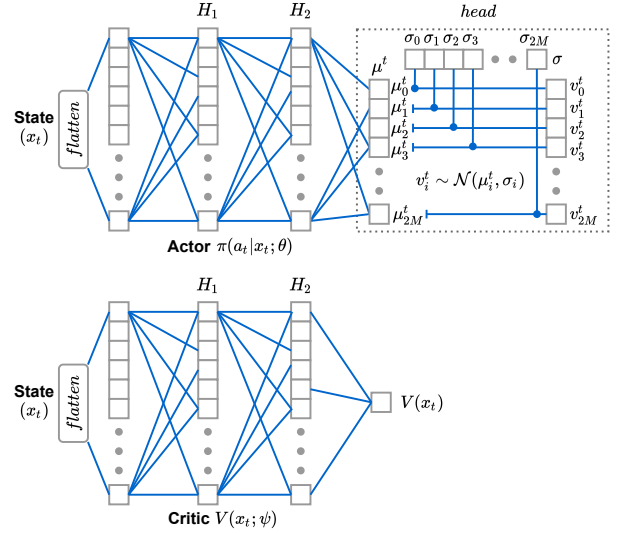


Fig. 2: Actor and Critic network architectures

The PPO-based scheduler leverages this voting mechanism, as shown in Fig. 2. At slot t , the actor network $\pi(a_t|x_t; \theta)$ outputs $2M$ normal distributions $\{\mathcal{N}(\mu_i^t, \sigma_i^t)\}_{i=1}^{2M}$ with mean $\mu^t = \{\mu_i^t\}_{i=1}^{2M}$ and standard deviation⁴ $\sigma = \{\sigma_i^t\}_{i=1}^{2M}$ to compute the votes as $\{v_i^t : v_i^t \sim \mathcal{N}(\mu_i^t, \sigma_i^t)\}_{i=1}^{2M}$. Thereafter, the votes are converted to $S_n(t) \forall n \in N$ and $\mathcal{U}(t)$ as per Eqns. (29) and (30), which are combined to obtain the final action a_t as given in Eqn. (27).

Algorithm 2 PPO-based scheduler

- 1: Initialize actor $\pi(a_t|x_t; \theta)$, critic $V(x_t; \psi)$
 - 2: Initialize actor's old parameters, $\theta_{old} \leftarrow \theta$
 - 3: **for** iteration $\leftarrow 1, 2 \dots \lceil \frac{T}{\epsilon \times T} \rceil$ **do**
 - 4: Replay Buffer $\mathcal{B} \leftarrow \{\}$
 - 5: **for** episode $\leftarrow 1, 2 \dots \mathcal{E}$ **do**
 - 6: **for** slot $t \leftarrow 0, 1, 2, \dots T-1$ **do**
 - 7: Observe current state x_t
 - 8: Execute action $a_t \sim \pi(\cdot|x_t; \theta_{old})$
 - 9: Observe next state x_{t+1} and, reward r_t
 - 10: Compute Advantage A_t using Eqn. (21)
 - 11: $\mathcal{B} \leftarrow \mathcal{B} \cup \{x_t, a_t, r_t, x_{t+1}, A_t\}$
 - 12: **for** epoch $\leftarrow 1, 2, \dots \eta$ **do**
 - 13: Sample minibatch $b_m \sim \mathcal{B}$ of size $|b_m| \leq E \times T$
 - 14: Compute gradients $\nabla_{\theta \cup \psi} \mathcal{L}(\theta \cup \psi)$ using Eqn. (25)
 - 15: Optimize parameters θ and ψ with the gradients:
 - 16: $\theta \leftarrow \theta - \alpha \nabla_{\theta} \mathcal{L}(\theta \cup \psi)$
 - 17: $\psi \leftarrow \psi - \alpha \nabla_{\psi} \mathcal{L}(\theta \cup \psi)$
 - 18: Update actor's old parameters, $\theta_{old} \leftarrow \theta$
-

4) *Algorithmic Description*: As shown in Algorithm 2, in the beginning, the PPO-based scheduler randomly initializes the parameters θ and ψ of the actor $\pi(\cdot)$ and critic $V(\cdot)$ networks, respectively (Line 1). It also initializes the actor's old parameters θ_{old} with θ (Line 2).

⁴Note that, PPO based scheduler explores the action space by increasing entropy $\mathcal{H}(\theta) = \frac{1}{2} \log(2\pi\sigma^2) + \frac{1}{2}$, see Eqn. (25).

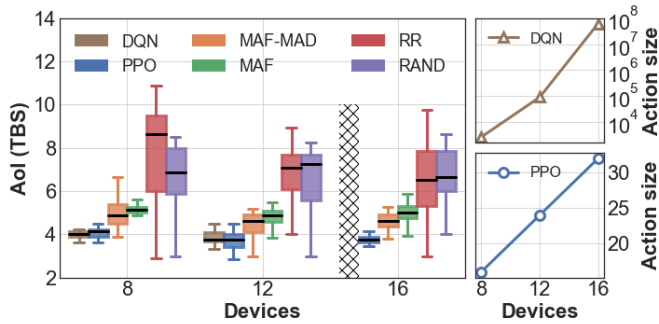


Fig. 3: Scalability of DQN vs PPO-based scheduler.

Next, the replay buffer \mathcal{B} is (re)initialized to store new experiences (Line 4). Following it, the actor interacts with the environment for \mathcal{E} episodes, where each episode is of length T . At slot t of an episode, the actor and the critic network observes the state x_t . Note that, the actor network utilizes its old parameters θ_{old} to compute action a_t . Next, action a_t is executed in the environment, resulting transition to next state x_{t+1} and the PPO based scheduler receives reward r_t (Line 8-9). The critic network computes the value of the state $V(x_t; \psi)$ to estimate the advantage A_t of taking action a_t on state x_t using Eqn. (21) (Line 10). At this point, the PPO-based scheduler obtains a new experience $\{x_t, a_t, r_t, x_{t+1}, A_t\}$, which is stored in the replay buffer \mathcal{B} (Line 11). At the end of \mathcal{E} episodes, the replay buffer contains $\mathcal{E} \times T$ entries (Lines 12 - 18), which trains the actor and critic networks as discussed next.

A minibatch b_m is sampled from the replay buffer \mathcal{B} , where $|b_m| \leq \mathcal{E} \times T$. Subsequently, the gradient $\nabla_{\theta \cup \psi} \mathcal{L}(\theta \cup \psi)$ is computed on minibatch b_m using Eqn. (25). Next, the gradient (i) $\nabla_{\theta} \mathcal{L}(\theta \cup \psi)$ with respect to actor parameters θ , and (ii) $\nabla_{\psi} \mathcal{L}(\theta \cup \psi)$ with respect to critic parameters ψ is utilized for optimizing (gradient descent) θ and ψ , where α is the learning rate. These gradient updates improve the actor and critic parameters and the PPO based scheduler performs multiple such updates over η epochs on the replay buffer \mathcal{B} . At the end of η epochs (Line 17), the actor network's old parameters θ_{old} is updated with the new actor network parameters θ (Line 18), which will be utilized for interacting with the environment in the next iteration (See line 3). The PPO-based scheduler runs for $\lceil \frac{\mathbb{T}}{\mathcal{E} \times T} \rceil$ iterations (Line 3-18) that improves the actor network parameters θ over old parameters θ_{old} , where \mathbb{T} denotes the total simulation duration.

Note that the convergence of neural networks are difficult to analyze and strongly depends on the hyper-parameters used [40]. Selection of hyperparameters is a challenging task and therefore a reasonable set of hyperparameters is found by trying different values. Similar to [14], [18], [19], [27], we limit investigation of the algorithm's convergence to simulations, where the neural network converges under the hyper-parameters used. The results presented for the DQN and PPO scheduler are the values obtained after their convergence.

C. PPO-based scheduler vs DQN-based scheduler

The advantages of the PPO-based scheduler over the DQN-based scheduler proposed in our preliminary work [13] are:

a) *Smaller Action Size*: DQN suffers from performance issues in networks with larger action spaces [13]. The number of actions for the DQN-based scheduler is given by $(\prod_i^{m_i} C_L) \times {}^M C_K$, which means the action size increases rapidly as the network size increases and DQN *doesn't* provide satisfactory performance when the action size is very large [41]. Due to this, works involving DQN for scheduling in IoT networks to improve AoI have been limited to smaller networks [14], [18], [19], [21], [27]. This can be seen in Fig. 3 where we consider 3 different UAV-relayed IoT networks with $M = 8, 12$, and 16 IoT devices. Note that the number of UAV channels (L) is $\frac{m_n}{2}$ and TBS channels (K) is $\frac{M}{2}$ as it leads to the maximum possible actions (see Sec.IV-B2).

As shown in Fig. 3, the DQN-based scheduler sees a factorial increase in the action size, whereas the action size of PPO-based scheduler increases linearly as $2M$, twice the number of IoT devices M . While both DQN and PPO perform relatively well for the first two networks with $M = 8$ and 12 devices, the DQN-based approach is not feasible for $M = 16$ as its action size is of the order 10^8 (memory required is very large), whereas the PPO's action size is 32. This shows several folds improvement of PPO-based scheduler over DQN-based scheduler in reducing the action size, and thus, much better scalability of the PPO-based scheduler.

b) *Scheduler's Generalization ability*: In certain situations, the training and the deployment network conditions could be different, e.g., devices might change the periodicities or the channel qualities can change. Under such situations, it is desirable if a trained scheduler is able to adapt to the new environment faster than training a new scheduler from scratch. Because PPO is an on-policy algorithm, it is able to adapt. Whereas DQN is an off-policy algorithm which will always need a new scheduler to be trained every-time there is a change in the network conditions.

Consider a UAV-relayed IoT network E_1 with the parameters given in Table.II. Let us take two different networks, E_2 and E_3 both of which are similar to E_1 with the only difference mentioned in the following-

- In network E_2 , the channel conditions for 10% IoT devices and UAVs have changed with respect to E_1 ,
- In network E_3 the periodicity for 10% of IoT devices have changed with respect to E_1 .

In both E_2 and E_3 , a PPO-based scheduler will be trained from scratch to get the baseline performance and this will be termed as *uninitialized*. To showcase the ability of the PPO-based scheduler to generalize to a changed network environment, a PPO-based scheduler trained in E_1 will be deployed in E_2 and E_3 using 2 different approaches -

- explore*, meaning that scheduler trained for E_1 will be reused except for the actor head which will be re-trained;
- adapt*, meaning that scheduler trained for E_1 will be entirely reused including the actor head.

Note that, the actor head is comprised of the output layer of the actor network as shown in Fig. 2.

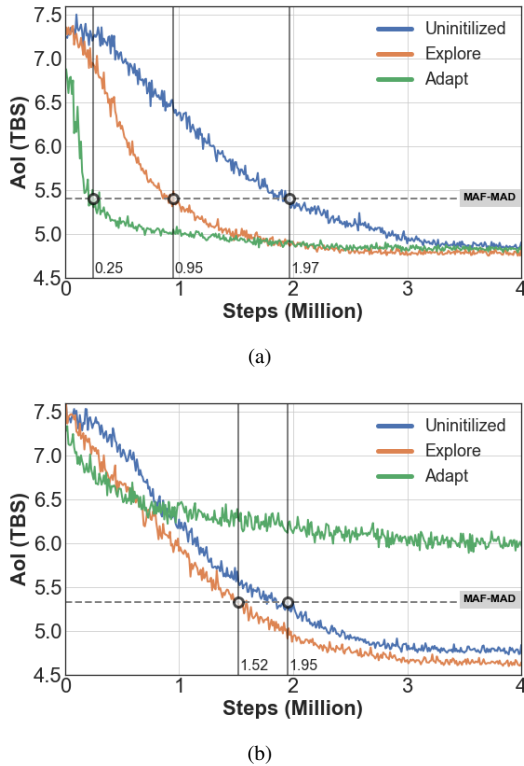


Fig. 4: Adaptability of the uninitialized, explore and adapt PPO-based schedulers with respect to changed (a) channel conditions (b) device periodicities. Here uninitialized refers to no pre-training, whereas the explore and adapt refers to pre-trained models with and without the actor head being retrained.

Fig. 4(a) shows the results for network E_2 . Both *explore* and *adapt* schedulers converge earlier than the *uninitialized*, with the *adapt* scheduler converging exceptionally fast. Therefore additional exploration to retrain the actor head doesn't lead to any benefit. However Fig. 4(b) shows the results for network E_3 where the *adapt* scheduler is unable to perform well and doesn't even outperform the MAF-MAD scheduler. Therefore re-training the actor head becomes important. The performance of the *uninitialized* and *adapt* schedulers are similar, signifying that the PPO-based scheduler generalizes well for changed channel conditions as compared to changed device periodicity.

V. RESULTS

This section discusses the performance evaluation of the proposed PPO-based scheduler against the baseline schedulers in terms of minimizing AoI at the TBS. The IoT devices and UAVs are placed randomly [29] in a simulation area of $l = b = 1000$ m and the observation interval $T = 20$ slots. Unless otherwise stated, we consider a general network setting with 30 IoT devices which are uniformly distributed among the 3 UAVs. The default parameters for the simulation study are listed in Table II. As discussed in previous section, because of the large memory requirements, it is not feasible for DQN-based scheduler to deal with general simulation setting (with > 12 IoT devices), we do not showcase the results for DQN-

based scheduler. Please refer to our preliminary paper [13] for results corresponding to smaller network scenarios.

The PPO-based scheduler (and DQN-based scheduler results presented in the previous section IV-C) are implemented on an NVIDIA DGX station with an Intel Xeon E5-2698 v4 CPU and an NVIDIA Tesla V100 GPU (32 GB memory). Data communication between CPU and GPU takes place through a PCIe 3.0 X16 slot. The hyper-parameters for DQN are kept the same as in [13], while the hyper-parameters for the PPO implementation are shown in Table III respectively.

TABLE II: Default network parameters

Number of IoT devices, M	30
Number of UAVs, N	3
IoT devices per UAV, m_n	(10, 10, 10)
Channels at each UAV, L	4
Channels at the TBS, K	10

TABLE III: PPO Hyper-parameters

Neurons in hidden layer 1 H_1	256
Neurons in hidden layer 2 H_1	256
Relay memory size $ \mathcal{B} $	2048
Minibatch size $ b_m $	512
Learning rate α	2.5×10^{-4}
Discount factor γ	0.99
Activation function	ReLU
Clip range ϵ	0.2
Optimizer	Adam
Epochs η	10
Total episodes \mathcal{E}	5×10^5

A. Baseline schedulers

- **Maximal AoI First (MAF) scheduler** – devices with highest AoI at both the UAV and TBS are selected for sampling and updating respectively [42]. For sampling, each UAV selects L devices with highest $AoI_m^{UAV}(t)$ out of the m_n devices associated to it. Similarly for updating, K devices out of the total M with highest $AoI_m^{TBS}(t)$ update their packets.
- **Deep-Q Network (DQN)-based scheduler** – this was proposed in our earlier work [13] and is based on a centralized DQN agent at the TBS.
- **Round Robin (RR) Scheduler** – under RR, the available channels are assigned in equal and circular fashion among the devices which ensures fairness among the devices [43]
- **Random scheduler** – A random set of devices are selected to be sampled and updated.

B. AoI Stacking

As shown in in Eqn. (26), the state space consists of the AoI of the devices stacked for previous z slots. A higher stack size provides more historical information at the expense of larger memory requirements. Here, Fig. 5 shows the AoI at the TBS achieved for different stack sizes. The convergence is initially faster with $z = 16$, but it takes more time to reach the optimal value. Whereas $z = 1$ converges very slowly. As, with higher stack size and increased information in the state, the parameters of the PPO-based scheduler increases as well.

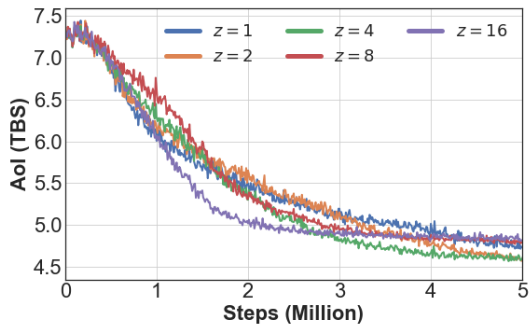


Fig. 5: Stack Size (z)

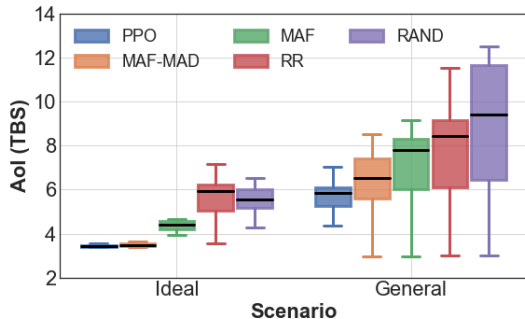


Fig. 6: Ideal vs general environment

Hence it takes less time to reach a considerable performance but struggles to fine tune itself against the environment. $z = 4$ provides a good trade-off between the convergence speed and the optimal performance. Thus the remaining experiments will utilize $z = 4$ slots for the state space⁵.

C. Ideal vs general environment

Ideal environments are characterized by lossless channels and generate-at-will traffic generation policy at the devices. The results shown in Fig. 6 confirm the analytical results derived in Theorem IV.1 that MAF-MAD is the optimal scheduling policy and outperforms all other scheduling policies under such ideal environments. As PPO is also able to learn the the optimal scheduling, it's performance also converges to MAF-MAD's performance. Overall, the PPO and MAF-MAD outperforms MAF, RR, random by 22.3%, 42.1%, 38.3% respectively. However when a general environment is considered where the ideal assumptions do not hold, MAF-MAD is no longer the optimal scheduler and PPO does better. It outperforms MAF-MAD, MAF, RR, random by 10.6%, 25.1%, 30.9%, 37.9% respectively. While the results could be shown for any channel condition and periodicities, they are pre-assigned for ease of reproducibility [13], [27], [36].

Note that the range of the AoI achieved by the PPO-based scheduler is much less than the other schedulers. The PPO-based scheduler considers the channel conditions while allocating resources. Therefore the devices with bad channels are scheduled more frequently so that their AoI do not suffer, at the expense of a higher AoI of the devices with better

⁵In our preliminary work [13], the DQN-based scheduler used stack size of $z = 1$.

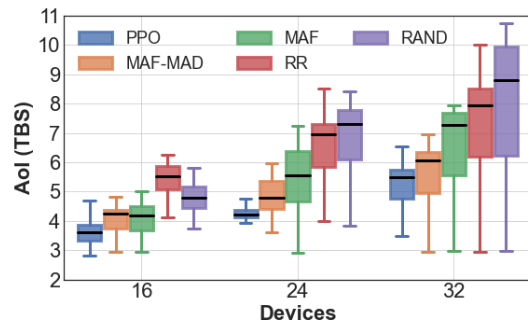


Fig. 7: AoI for varying number of IoT devices (M)

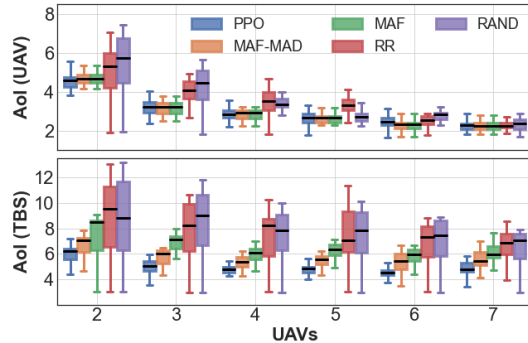


Fig. 8: AoI for varying number of UAVs (N)

channels. However for the other schedulers, the devices with good channels see a very low AoI and devices with bad channels will have high AoI, resulting in a higher range. This is because unlike our PPO-based scheduler, the counterpart schedulers do not have the ability to learn the various channel conditions/fluctuations.

For the rest of the experiments below, general conditions with lossy channels and periodic packet generation at the IoT devices are considered.

D. Effectiveness of PPO-based scheduler

In this section, we analyze the effectiveness of the PPO-based scheduler in minimizing the AoI at the TBS with changing network parameters such as the number of IoT devices, UAVs, UAV channels and TBS channels.

a) *Varying number of IoT devices (M):* As shown in Fig. 7, the PPO-based scheduler outperforms the baselines in all considered scenarios by a significant improvement of AoI at the TBS. However, an upward trend in the AoI can be observed as we increase the number of IoT devices in the network. The primary reason is the constant sampling and updating capacity of the network. Therefore, the increase of IoT devices results in less frequent sampling and updating of packets from a particular IoT device. Thus, we observe an increased average AoI at the TBS for all schedulers.

b) *Varying number of UAVs (N):* The PPO-based scheduler shows superiority in minimizing AoI at TBS with changing the number of UAVs in the network, see Fig. 8. As shown in the figure, the AoI at UAV is improved with more UAVs, which directly improves the AoI at the TBS as per Eqn (5). However, after a point, all schedulers show equivalent AoI

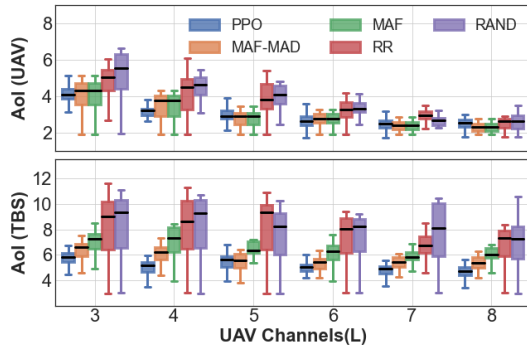


Fig. 9: AoI for varying UAV Channels (L)

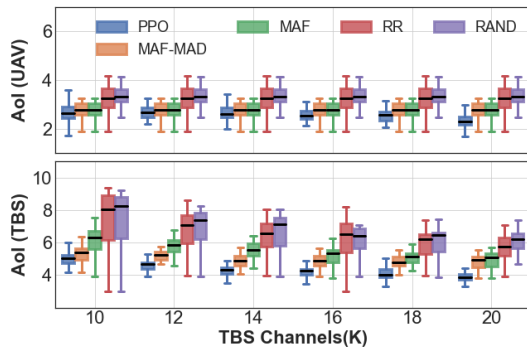


Fig. 10: AoI for varying TBS Channels (K)

at the UAV as most IoT devices can be sampled at once, and there is little scope of improvement due to scheduling. Despite similar AoI at the UAV, the PPO-based scheduler outperforms the baselines and improves the AoI further as it employs better scheduling decisions at the TBS.

c) *Varying number of UAV channels (L):* The increasing number of UAV channels has a similar effect to increasing the number of UAVs. For both ways, the sampling capacity of the network is improved. Hence, the AoI at the UAV improves up to a point when most of the IoT devices can be sampled at once and then becomes equivalent for all schedulers, see Fig. 9. Nevertheless, the PPO-based scheduler outperforms the baselines in minimizing the AoI at the TBS in all considered scenarios. Note that the PPO-based scheduler achieves a 61.8% improvement in AoI at the UAV with increased UAV channels from 3 to 8. However, all this gain is not transferable to the TBS, and it only sees a 23.7% improvement in the AoI due to the bottleneck at UAV to TBS communication.

d) *Varying number of TBS channels (K):* On the contrary, increasing the number of TBS channels does not change the sampling capacity of the network. Thus, the AoI at the UAV remains unchanged for a particular scheduler with the increase of 10 to 20 in TBS channels, see Fig. 10. Instead, the network’s updating capacity is improved, allowing more packets to be transferred from the UAVs to the TBS. Therefore, the TBS sees a 31.0% improvement in AoI for PPO-based scheduling and outperforms the baselines. Thus, the channels between the UAVs and the TBS (K) are more critical bottlenecks than the channels between IoT devices and the UAVs (L) in minimizing AoI at the TBS.

VI. CONCLUSION

We propose a Maximal Age First - Maximal Age Difference (MAF-MAD) scheduler and prove its optimality in improving AoI in a UAV-relayed IoT network with two hops, where the UAVs act as static aerial base station (ABS) that relay packets between the IoT devices and the terrestrial base station (TBS) under no packet loss in any of the channels and generate-at-will traffic generation model at the IoT devices. However when packet loss in the channels and periodicity in packet generation by the IoT devices are considered, MAF-MAD scheduler is no longer optimal. Therefore we propose a Proximal Policy Optimization (PPO)-based scheduler which performs better than the MAF-MAD scheduler under such realistic general conditions. We also show that the channels between the UAVs and the TBS play a much important role in improving AoI at the TBS compared to channels between the IoT devices and UAV, which points to the importance of backhaul links compared to access links for AoI minimization. In our future work, we will consider mobility and optimal UAV placement under UAV-relayed IoT networks with the objective of improving information freshness at the TBS.

REFERENCES

- [1] J.-M. Martinez-Caro and M.-D. Cano, “Iot system integrating unmanned aerial vehicles and lora technology: a performance evaluation study,” *Wireless Communications and Mobile Computing*, vol. 2019, 2019.
- [2] F. Luo, C. Jiang, S. Yu, J. Wang, Y. Li, and Y. Ren, “Stability of cloud-based uav systems supporting big data acquisition and processing,” *IEEE Transactions on Cloud Computing*, vol. 7, no. 3, pp. 866–877, 2019.
- [3] N. S. Solutions, “How Las Vegas is using data to boost public safety - Cities Today - Connecting the world’s urban leaders,” <https://cities-today.com/industry/las-vegas-data-boost-public-safety/>, (Accessed on 12/27/2020).
- [4] M. Costa, M. Codreanu, and A. Ephremides, “On the age of information in status update systems with packet management,” *IEEE Transactions on Information Theory*, vol. 62, no. 4, pp. 1897–1910, 2016.
- [5] S. Kaul, M. Gruteser, V. Rai, and J. Kenney, “Minimizing age of information in vehicular networks,” in *2011 8th Annual IEEE Communications Society Conference on Sensor, Mesh and Ad Hoc Communications and Networks*, 2011, pp. 350–358.
- [6] R. D. Yates, Y. Sun, D. R. Brown, S. K. Kaul, E. Modiano, and S. Ulukus, “Age of information: An introduction and survey,” *IEEE Journal on Selected Areas in Communications*, vol. 39, no. 5, pp. 1183–1210, 2021.
- [7] “The Ongoing History of the Age of Information,,” <http://webhome.auburn.edu/~yzs0078/AoI.html>, (Accessed on 06/04/2021).
- [8] H. Hu, K. Xiong, G. Qu, Q. Ni, P. Fan, and K. B. Letaief, “Aoi-minimal trajectory planning and data collection in uav-assisted wireless powered iot networks,” *IEEE Internet of Things Journal*, vol. 8, no. 2, pp. 1211–1223, 2021.
- [9] B. Choudhury, V. K. Shah, A. Dayal, and J. H. Reed, “Joint age of information and self risk assessment for safer 802.11p based v2v networks,” in *IEEE INFOCOM 2021 - IEEE Conference on Computer Communications*, 2021, pp. 1–10.
- [10] X. Wang, C. Chen, J. He, S. Zhu, and X. Guan, “Aoi-aware control and communication co-design for industrial iot systems,” *IEEE Internet of Things Journal*, vol. 8, no. 10, pp. 8464–8473, 2021.
- [11] B. Choudhury, V. K. Shah, A. Dayal, and J. H. Reed, “Experimental analysis of safety application reliability in v2v networks,” in *2020 IEEE 91st Vehicular Technology Conference (VTC2020-Spring)*, 2020.
- [12] A. Aziz, K. Singh, W. Osamy, and A. M. Khedr, “Effective algorithm for optimizing compressive sensing in iot and periodic monitoring applications,” *Journal of Network and Computer Applications*, vol. 126, pp. 12–28, 2019.
- [13] B. Choudhury, V. K. Shah, A. Ferdowsi, J. H. Reed, and Y. T. Hou, “Aoi-minimizing scheduling in uav-relayed iot networks,” in *2021 IEEE 18th International Conference on Mobile Ad Hoc and Smart Systems (MASS)*, 2021, pp. 117–126.

- [14] M. A. Abd-Elmagid, A. Ferdowsi, H. S. Dhillon, and W. Saad, "Deep reinforcement learning for minimizing age-of-information in uav-assisted networks," in *2019 IEEE Global Communications Conference (GLOBECOM)*. IEEE, 2019, pp. 1–6.
- [15] G. Ahani, D. Yuan, and Y. Zhao, "Age-optimal uav scheduling for data collection with battery recharging," *IEEE Communications Letters*, vol. 25, no. 4, pp. 1254–1258, 2021.
- [16] T. Wu, J. Liu, J. Liu, Z. Huang, H. Wu, C. Zhang, B. Bai, and G. Zhang, "A novel ai-based framework for aoi-optimal trajectory planning in uav-assisted wireless sensor networks," *IEEE Transactions on Wireless Communications*, pp. 1–1, 2021.
- [17] J. Liu, X. Wang, B. Bai, and H. Dai, "Age-optimal trajectory planning for uav-assisted data collection," in *IEEE INFOCOM 2018-IEEE Conference on Computer Communications Workshops (INFOCOM WKSHPs)*. IEEE, 2018, pp. 553–558.
- [18] J. Hu, H. Zhang, K. Bian, L. Song, and Z. Han, "Distributed trajectory design for cooperative internet of uavs using deep reinforcement learning," in *2019 IEEE Global Communications Conference (GLOBECOM)*, 2019, pp. 1–6.
- [19] C. Zhou, H. He, P. Yang, F. Lyu, W. Wu, N. Cheng, and X. Shen, "Deep rl-based trajectory planning for aoi minimization in uav-assisted iot," in *2019 11th International Conference on Wireless Communications and Signal Processing (WCSP)*. IEEE, 2019, pp. 1–6.
- [20] S. Zhang and R. Zhang, "Trajectory optimization for cellular-connected uav under outage duration constraint," *Journal of Communications and Information Networks*, vol. 4, no. 4, pp. 55–71, 2019.
- [21] J. Hu, H. Zhang, L. Song, R. Schober, and H. V. Poor, "Cooperative internet of uavs: Distributed trajectory design by multi-agent deep reinforcement learning," *IEEE Transactions on Communications*, 2020.
- [22] M. Yi, X. Wang, J. Liu, Y. Zhang, and B. Bai, "Deep reinforcement learning for fresh data collection in uav-assisted iot networks," in *IEEE INFOCOM 2020 - IEEE Conference on Computer Communications Workshops (INFOCOM WKSHPs)*, 2020, pp. 716–721.
- [23] D. Chen, "Energy-efficient uav-sensor data harvesting: Dynamic adaptive modulation and height control," *arXiv preprint arXiv:2201.12142*, 2022.
- [24] B. Buyukates, A. Soysal, and S. Ulukus, "Age of information in two-hop multicast networks," in *2018 52nd Asilomar Conference on Signals, Systems, and Computers*. IEEE, 2018, pp. 513–517.
- [25] A. Arafa and S. Ulukus, "Timely updates in energy harvesting two-hop networks: Offline and online policies," *IEEE Transactions on Wireless Communications*, vol. 18, no. 8, pp. 4017–4030, 2019.
- [26] M. Moradian and A. Dadlani, "Age of information in scheduled wireless relay networks," in *2020 IEEE Wireless Communications and Networking Conference (WCNC)*. IEEE, 2020, pp. 1–6.
- [27] J. Song, D. Gunduz, and W. Choi, "Optimal scheduling policy for minimizing age of information with a relay," *arXiv preprint arXiv:2009.02716*, 2020.
- [28] R. Han, Y. Wen, L. Bai, J. Liu, and J. Choi, "Age of information aware uav deployment for intelligent transportation systems," *IEEE Transactions on Intelligent Transportation Systems*, pp. 1–11, 2021.
- [29] J. Lyu, Y. Zeng, R. Zhang, and T. J. Lim, "Placement optimization of uav-mounted mobile base stations," *IEEE Communications Letters*, vol. 21, no. 3, pp. 604–607, 2016.
- [30] "How IoT Short-Range Connectivity Stacks Up — Mouser," <https://www.mouser.com/applications/home-automation-how-iot-short-range-stacks-up/>, (Accessed on 05/29/2021).
- [31] Z. Xi, Y. Zhou, D. Zhang, J. Wang, S. Chen, Y. Wang, X. Li, H. Wang, and J. Wu, "Hypergen: High-performance flexible packet generator using programmable switching asic," in *Proceedings of the ACM SIGCOMM 2019 Conference Posters and Demos*, 2019, pp. 42–44.
- [32] C. Saha, H. S. Dhillon, N. Miyoshi, and J. G. Andrews, "Unified analysis of hetnets using poisson cluster processes under max-power association," *IEEE Transactions on Wireless Communications*, vol. 18, no. 8, pp. 3797–3812, 2019.
- [33] J. Sabzehali, V. K. Shah, H. S. Dhillon, and J. H. Reed, "3d placement and orientation of mmwave-based uavs for guaranteed los coverage," *IEEE Wireless Communications Letters*, pp. 1–1, 2021.
- [34] P. Li and J. Xu, "Placement optimization for uav-enabled wireless networks with multi-hop backhauls," *Journal of Communications and Information Networks*, vol. 3, no. 4, pp. 64–73, 2018.
- [35] D. Tse and P. Viswanath, *Fundamentals of wireless communication*. Cambridge university press, 2005.
- [36] C. Li, Y. Huang, Y. Chen, B. Jalaian, Y. T. Hou, and W. Lou, "Kronos: A 5g scheduler for aoi minimization under dynamic channel conditions," in *2019 IEEE 39th International Conference on Distributed Computing Systems (ICDCS)*, 2019, pp. 1466–1475.
- [37] C. J. Watkins and P. Dayan, "Q-learning," *Machine learning*, vol. 8, no. 3-4, pp. 279–292, 1992.
- [38] J. Schulman, S. Levine, P. Abbeel, M. Jordan, and P. Moritz, "Trust region policy optimization," in *International conference on machine learning*. PMLR, 2015, pp. 1889–1897.
- [39] J. Schulman, F. Wolski, P. Dhariwal, A. Radford, and O. Klimov, "Proximal policy optimization algorithms," *arXiv preprint arXiv:1707.06347*, 2017.
- [40] H. S. Jomaa, J. Grabocka, and L. Schmidt-Thieme, "Hyp-rl: Hyperparameter optimization by reinforcement learning," *arXiv preprint arXiv:1906.11527*, 2019.
- [41] T. Zahavy, M. Haroush, N. Merlis, D. J. Mankowitz, and S. Mannor, "Learn what not to learn: Action elimination with deep reinforcement learning," *arXiv preprint arXiv:1809.02121*, 2018.
- [42] Y. Sun, E. Uysal-Biyikoglu, and S. Kompella, "Age-optimal updates of multiple information flows," in *IEEE INFOCOM 2018-IEEE Conference on Computer Communications Workshops (INFOCOM WKSHPs)*. IEEE, 2018, pp. 136–141.
- [43] C. F. Müller, G. Galaviz, Á. G. Andrade, I. Kaiser, and W. Fengler, "Evaluation of scheduling algorithms for 5g mobile systems," in *Computer Science and Engineering—Theory and Applications*. Springer, 2018, pp. 213–233.